Long-Distance Terahertz Single-Photon 3-D Imaging Based on Scaling Training

Chuanying Liang, Chenggao Luo, Jun Yi, Bin Deng, Hongqiang Wang, Kang Liu, and Qi Yang

***Abstract*—In this article, to address the long-distance imaging problems, a novel forward-looking 3-D imaging method based on terahertz single-photon radar is presented. The imaging method is based on single-input and single-output architecture system and adopts a novel data-driven approach named scaling training. In the scaling training, by scaling the parameters of the long-distance scene to be imaged, a parameter scaling system is constructed, and then it is utilized to collect the training data to train the artificial neural network (ANN) model. Once the training is completed, 3-D image of the long-distance scene can be retrieved using the ANN model from solely the 1-D photon-counting histogram echo recorded by terahertz single-photon radar. On the basis, to further improve the imaging quality, the depth correction method is implemented. Finally, numerical simulations are carried out to demonstrate the feasibility of the proposed method.**

***Index Terms*—Data-driven, forward-looking 3-D imaging, single-photon radar, terahertz radar.**

I. Introduction

As an effective approach to acquire spatial information, radar imaging has aroused great concern [1], [2], [3], [4]. Since the electromagnetic spectrum of terahertz waves lie between the microwave and infrared, terahertz radar has higher resolution over microwave radar [5], and stronger penetration capability over lidar [6], [7]. Thus, it is has great potential in many military and civil applications [3]. However, the operation range is limited by the significant atmospheric attenuation and great challenge of high-power radiation technology in terahertz band, the state-of-art terahertz radar system can only operate at a distance of up to 4 km [8]. To further improve the operation range of terahertz radar, the research on terahertz single-photon detector with single-photon response sensitivity is developing rapidly [9], [10], [11], [12], [13], its combination with terahertz radar is terahertz single-photon radar [14], [15].

In the past decades, single-photon radar imaging is mainly implemented in optics field, and most works are based on detector arrays or mechanical scanning [16], [17], [18], [19]. But for terahertz band, since the photon energy is much lower, the terahertz single-photon detector requires additional refrigeration equipment with large volume and high power consumption, which significantly increases the technical difficulty of expanding the terahertz single-photon detector into large-format arrays. In addition, the diffraction effect of terahertz wave imposes additional difficulties for designing quasi-optical scanning systems. Although there is a data-driven 3-D imaging method based on single-input and single-output (SISO) terahertz single-photon radar for retrieving the 3-D image [20], [21], the terahertz single-photon radar is often implemented in long-distance applications and the training step of the imaging method requires huge amounts of data. Moreover, in long-distance applications, data collection will be a thorny issue since the target is usually noncooperative. Thus, this article focuses on the research of long-distance 3-D imaging method based on terahertz single-photon radar.

To address the issue mentioned above, we demonstrate a novel 3-D imaging method based on SISO terahertz single-photon radar. Only the arrival time of the return photons from the whole scene in the form of a photon-counting histogram is recorded, and a parameter scaling system, which is constructed by scaling the parameters of the long-distance scene to be imaged, is utilized to collect the training data. Then, the training data are devoted to train the artificial neural network (ANN) model. Finally, the ANN model is utilized to reconstruct the 3-D image of the long-distance scene from a single photon-counting histogram. The employed radar imaging system is compact and cost-effective, which does not rely on detector arrays or mechanical scanning. In addition, benefited from the data-driven approach, real-time imaging is entirely possible to be realized. The contribution of this article can be summarized as follows.

1) We proposed a method named scaling training to solve the long-distance 3-D imaging problem of terahertz single-photon radar.
2) The principle of scaling training is derived from the formula, and in the simulations, we analyzed the influence on imaging quality by the ratio of different pulse width to time bin and different pulse accumulation times.
3) To further improve the imaging quality, we proposed a depth correction method and demonstrated its feasibility by simulations.

The rest of this article is organized as follows. In Section II, theoretical analysis of the imaging problem is discussed, and the corresponding 3-D imaging method is introduced. Numerical

Manuscript received 12 July 2023; revised 31 August 2023, 17 October 2023, and 17 November 2023; accepted 27 November 2023. Date of publication 30 November 2023; date of current version 20 December 2023. This work was supported in part by the National Natural Science Foundation of China under Grant 61971427, Grant 62035014, Grant 61921001, Grant 62201591, and Grant 62105356, and in part by the National Key R&D Program of China under Grand 2018YFB2202500 and Grand 2022YFB3902400. *(Corresponding authors: Chenggao Luo; Jun Yi.)*

The authors are with the College of Electronic Science and Technology, National University of Defense Technology, Changsha 410073, China (e-mail: 15871181540@163.com; luochenggao@nudt.edu.cn; yijun@nudt.edu.cn; dengbin@nudt.edu.cn; wanghongqiang@nudt.edu.cn; liukang1117@126.com; yangqi08@nudt.edu.cn).

Digital Object Identifier 10.1109/JSTARS.2023.3338008

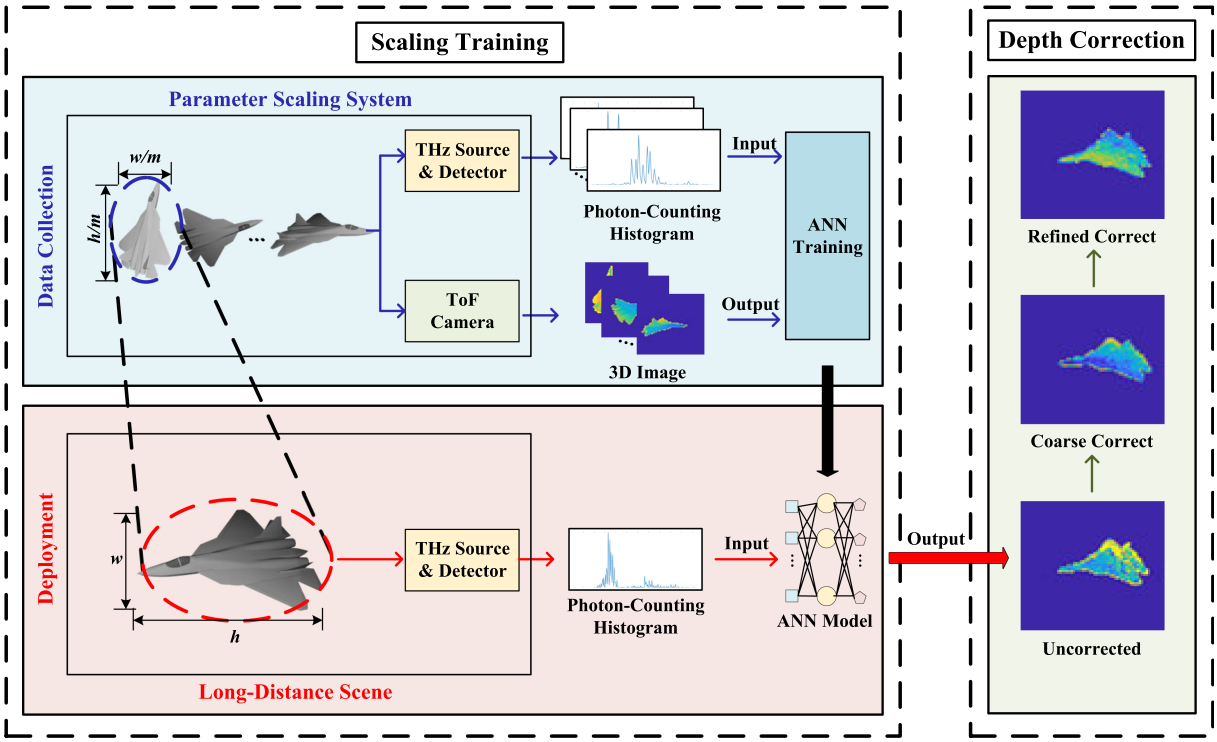

Fig. 1. Proposed 3-D imaging method.

simulations are performed in Section III to demonstrate the feasibility of the proposed method. In Section IV, a depth correction algorithm is proposed to improve the imaging quality of the method presented in Section III. Finally, Section V concludes this article.

II. Principle of the Proposed Method

A. System Architecture and Imaging Principle

The schematic of the proposed 3-D imaging method is shown in Fig. 1. It mainly includes two processes, that is, the scaling training and depth correction. In the scaling training, the data collection is implemented in a parameter scaling system, which is constructed by scaling the parameters of the long-distance scene to be imaged according to specific rules. In the parameter scaling system, a terahertz single-photon radar records the arrival time of the return photons from the whole scene in the form of a photon-counting histogram, in parallel, a time-of-flight (TOF) camera [22], [23] is used to record the 3-D images of the scene. The 3-D images are displayed as depth maps, in which the depth is encoded by different colors. The attitude and position of the target are constantly changing during the data collection process to obtain a large amount of data. Then, by taking the photon-counting histogram as the input and the 3-D images as the output, the ANN model is trained to find the implied mapping between the photon-counting histogram and the 3-D scene. Due to the existence of parameters scaling, this is similar to the mapping in the long-distance scene. Once the training is completed, in the deployment step, the 3-D image of real target can be retrieved only from the photon-counting histogram of using the ANN model. The second step is depth correction, it is aimed at addressing the imprecise depth information inversion in scaling training method. The depth correction method includes two steps named coarse correction and refined correction, and will be detailed in Section IV.

B. 3-D Imaging With Ill-Posed Problem

The proposed 3-D imaging scheme mentioned above is based on a SISO terahertz single-photon radar, and the echo of the 3-D scene is 1-D photon-counting histogram. Thus, the high-dimensional spatial information is compressed into low-dimensional representation, which inevitably leads to the loss of useful information. As a result, the 3-D imaging problem becomes strongly ill-posed. Data-driven approaches, especially ANN, have shown great application potential in solving ill-posed problems of high-dimensional information inversion [24]. ANN can reveal the implicit mapping between high-dimensional spatial information and low-dimensional representation, and then retrieve the spatial information from inverse mapping.

Previous work has shown that, the MLP model, a classic forward-structured ANN used in various fields [25], [26], indicating great potential in retrieving 3-D images from range profile, i.e., the 1-D range information of the scene [27]. On the one hand, the photon-counting histogram essentially represents the 1-D range information of the 3-D scene, thus, it is possible to utilize the MLP model retrieve 3-D image from photon-counting histogram. On the other hand, the energy of each time bin in the photon-counting histogram is contributed by all the scattering points on the target of the same distance from the detector.

TABLE I
PARAMETERS OF LONG-DISTANCE SCENE AND ITS PARAMETER SCALING SYSTEM

Parameter \ category	Long-distance scene	Parameter scaling system
Range	R	R/m
Transmitting power	P	P/m^4
Pulse width	T_{p}	T_{p}/m
Time bin	t_{s}	t_{s}/m
Range gate	T_{g}	T_{g}/m
Image plane size	$s_1 \times s_2$	$(s_1/m) \times (s_2/m)$
Target size	$w \times d \times l$	$(w/m) \times (d/m) \times (l/m)$

Therefore, each bin of the input photon-counting histogram is related to all the pixels of the output 3-D image, and this character conforms the structure of the MLP model. Hence, MLP is selected to solve the problem of ill-posed image inversion.

C. Scaling Training

Here, we introduce the principle of scaling training and derive it with formula. Assume that the range of long-distance scene to be imaged is *R*, transmitting power of terahertz source is *P*, pulse width of the transmitting terahertz pulse is T_{p}, the time bin of the terahertz single-photon detector is t_{s}, the width of the range gate is T_{g}, and the scaling factor is *m*. Based on that, the parameters of the scaling system are listed in Table I.

The terahertz single-photon radar is regarded as the origin, assume that there is a target point at range *R*, the transmitting signal is in the form of

$$E(t) = Au(t)\mathrm{e}^{\mathrm{j}2\pi\nu t} \tag{1}$$

where *A* is the signal magnitude, $u(t)$ is the signal envelope, j is the imaginary unit, and ν denotes the signal frequency. In general, $u(t)$ is denoted as

$$u(t) = \sqrt{\frac{t}{\tau}\mathrm{e}^{-\frac{t}{\tau}}} \tag{2}$$

where τ is a constant related to pulse width. According to radar equation [28], the echo signal can be deduced as

$$S(t) = K_{\mathrm{s}}\frac{A}{R^2}\sqrt{\frac{(t-t_0)}{\tau}\mathrm{e}^{-\frac{(t-t_0)}{\tau}}}\mathrm{e}^{\mathrm{j}2\pi\nu(t-t_0)} \tag{3}$$

where t_0 and K_{s} represent the time delay and a constant, which are defined by

$$t_0 = \frac{2R}{c} \tag{4}$$

$$K_{\mathrm{s}} = \sqrt{\frac{G_{\mathrm{t}}\alpha_{\mathrm{t}}^2\sigma A_{\mathrm{e}}\rho}{(4\pi)^2 L}} \tag{5}$$

respectively. Where c is the speed of light, G_{t} is the gain of transmitting antenna, α_{t} is the attenuation coefficient of atmospheric propagation, σ is the radar cross section, A_{e} is the effective aperture of receiving antenna, ρ is the aperture efficiency, and L is the radar system loss.

Based on the abovementioned conditions, a parameter scaling system can be constructed. Assume that there is a target point in the parameter scaling system at range R/m, the transmitting signal is represented by

$$E_{\mathrm{sca}}(\eta) = A_{\mathrm{sca}}u_{\mathrm{sca}}(\eta)\mathrm{e}^{\mathrm{j}2\pi\nu\eta} \tag{6}$$

where A_{sca} and $u_{\mathrm{sca}}(\eta)$ are the signal magnitude and signal envelop, respectively. According to Table I, the transmitting power and pulse width are scaled to P/m^4 and T_{p}/m, respectively. Thus, we obtain

$$A_{\mathrm{sca}} = \frac{A}{m^2} \tag{7}$$

$$u_{\mathrm{sca}}(\eta) = \sqrt{\frac{\eta}{\tau/m}\mathrm{e}^{-\frac{\eta}{\tau/m}}}. \tag{8}$$

Combining (7), (8), and radar equation, the echo signal of the point target in the parameter scaling system can be deduced as

$$S_{\mathrm{sca}}(\eta) = K_{\mathrm{s}}\frac{A}{R^2}\sqrt{\frac{(\eta-t_0/m)}{\tau/m}\mathrm{e}^{-\frac{(\eta-t_0/m)}{\tau/m}}}\mathrm{e}^{\mathrm{j}2\pi\nu(\eta-t_0/m)}. \tag{9}$$

On the other hand, in view of the range gate is scaled to T_{g}/m and the time bin is scaled to t_{s}/m, the relationship of the time variable between the long-distance scene to be imaged and the parameter scaling system can be deduced as

$$\eta = \frac{t}{m} \tag{10}$$

substituting (10) into (9), we have

$$S_{\mathrm{sca}}(t) = K_{\mathrm{s}}\frac{A}{R^2}\sqrt{\frac{(t-t_0)}{\tau}\mathrm{e}^{-\frac{(t-t_0)}{\tau}}}\mathrm{e}^{\mathrm{j}\frac{2\pi\nu(t-t_0)}{m}}. \tag{11}$$

Comparing $S(t)$ with $S_{\mathrm{sca}}(t)$, it is clear that the echo signal of the long-distance scene to be imaged and parameter scaling system have the same magnitude and envelope, which means that the photon-counting histograms of these two have similar mapping relationship with the corresponding 3-D scene. Above all is the theoretical analysis of the scaling training method.

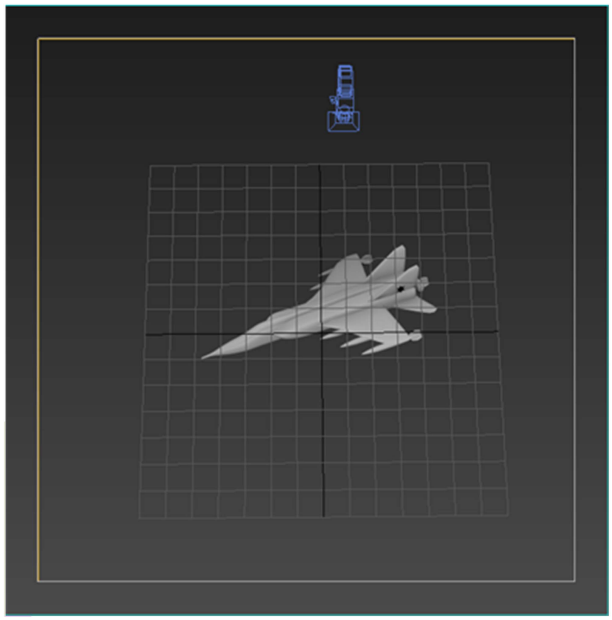

Fig. 2. Virtual scene to get 3-D images in 3-Ds Max 2020.

III. Numerical Simulations

In this section, simulations are carried out to demonstrate the feasibility of the proposed method.

A. Simulations Set-Up

The set-up is shown as Fig. 1. The data collection step is implemented in the parameter scaling system. The virtual 3-D imaging scene is a 3-D plane target with clear sky background, and the plane moves in a fixed field of view (i.e., imaging plane), while the posture and position of the plane are constantly changing to generate the required amount of data.

As shown in Fig. 2, the simulation data collection is performed in 3-Ds Max 2020. After the 3-D plane model is imported into the scene, a light that attenuates with the square of the range is directly set above the imaging plane to cover the model. Then, control the motion track of the plane and change its rotation angle, translation direction, and type. The 3-D images of the plane are obtained by projecting them along the line-of-sight direction of the TOF camera, where the depth is presented by the color of the pixels. Meanwhile, 1-D photon-counting histograms of the corresponding scenes are obtained to construct dataset.

Here, there are three different types of 3-D plane targets in the dataset, and the position transformation and rotation transformation are carried out along three different axes. Some plane types and attitude pictures in the dataset are shown in Fig. 3. The 3-D depth images and their corresponding photon-counting histogram are paired to form the dataset, which contains 6000 groups of imaging data. Then, the dataset is utilized to train the MLP model, the MLP is composed of five layers: an input layer, three fully connected layer (with 1024, 512, 256 nodes, respectively) and an output layer (with 4096 nodes), and there is a activation function (tanh in our case) after each fully connected layer. Training is performed in Python 3.8 using Pytorch 1.6.0 on a laptop equipped with a Intel Core i7 Eight Core Processor i7-7700HQ CPU at 2.80 GHz. The training time in our condition is 140 min in total (the number of images is 5400, batch size is 16, and the number of epochs is 500). After training the model, we can recover a 3-D image from a single photon-counting histogram in 20 ms on our laptop. During learning process, the loss is calculated by mean square error, and the optimizer employed is the Adam optimizer.

B. Simulation Results

Next, numerical simulations of two kinds of parameters are performed. One of the long-distance scene is set at 10 km, and the corresponding parameter scaling system is set at 200 m, while the parameters of the other one are set at 100 km and 2 km, respectively. The size of the plane target is set according to the size of the real fighter, about 40 m $\times$ 40 m $\times$ 10 m. The specific parameters of the 10 km simulations is listed in Table II, while the parameters of the 100 km simulations are the same with Table II except range.

After training the MLP model, the photon-counting histograms of 10 km and 100 km scenes are simulated and taken as the input, then the output is regarded as the retrieved 3-D images. The corresponding 3-D imaging results are shown in Figs. 4 and 5.

In Fig. 4, there are four group of imaging results. The leftmost column shows the 3-D plane targets, the second column presents the photon-counting histograms of the plane target under the simulation parameters in Table II, the third column gives the corresponding 3-D depth images, and the rightmost column demonstrates the images retrieved by the MLP model trained by the data of parameter scaling system. From the four sets of imaging results, it can be seen that the proposed method is more accurate for the inversion of contour information. Although the inversion accuracy of internal depth information is slightly low, it can still reflect the structural characteristics and depth changes of the 3-D plane target. The reason why the depth information inversion is not accurate is that when the data of parameter scaling system is used for training the MLP, the depth information inversion error may be in the order of centimeter to decimeter. When utilized in long-distance scenes, as the distance is magnified by 50 times, the error will also be magnified by 50 times, resulting in an error of meter magnitude. However, considering that the imaging system is implemented in a SISO imaging system without scanning, and the target size at 10 km away is about 40 m $\times$ 40 m $\times$ 20 m, thus, the error of meter magnitude is within the tolerance range. In the four sets of imaging results, the inversion results of different target types, different attitudes and angles are displayed, which obviously demonstrates the effectiveness and reliability of the proposed method. It is noteworthy that two different setting in scattering coefficient of the targets are taken into consideration, i.e., all the points are set to 1 and all the points are set randomly. However, the difference between the them did not have a significant impact on the results, thus, without losing generality, the scattering coefficient of the target point in all simulations in this article is set to 1.

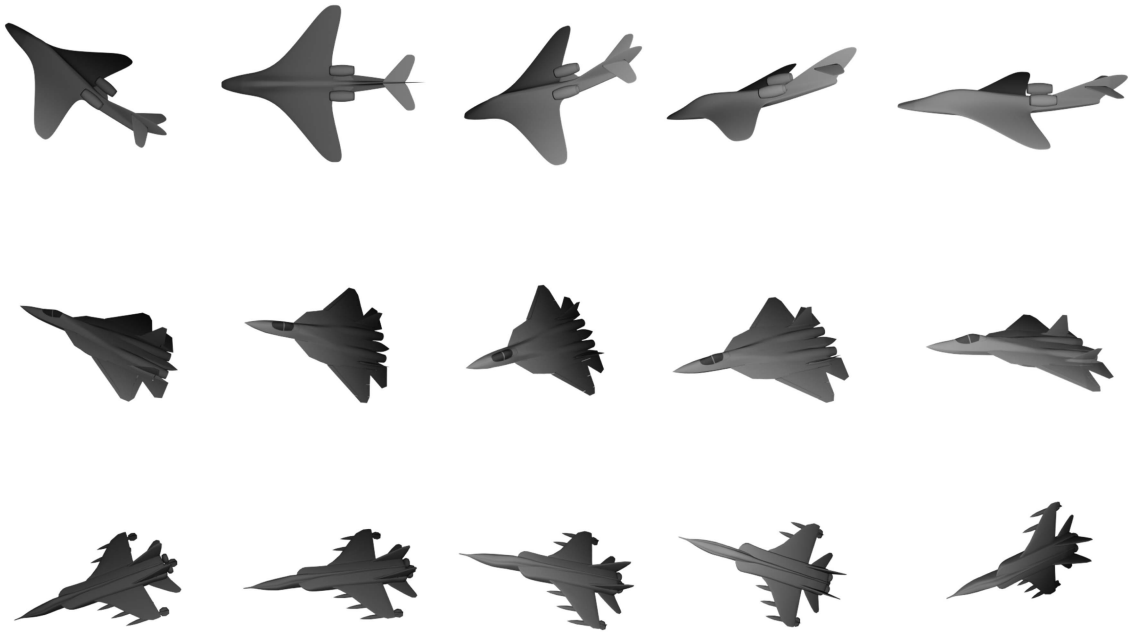

Fig. 3. Attitude of some plane targets in dataset.

TABLE II
PARAMETERS OF THE NUMERICAL SIMULATIONS

Parameter	Parameter scaling system	Long-distance scene
Frequency	4.3 THz	4.3 THz
Pulse width	1 ps	50 ps
Time bin	1 ps	50 ps
Range gate	8 ns	400 ns
Detect efficiency	25%	25%
Noise photons rate	1.25 MHz	1.25 MHz
Pulse accumulation times	10000	10000
Imaging plane	1.28 m × 1.28 m	64 m × 64 m
Imaging pixels	64 × 64	64 × 64
Range	200 m	10000 m
Target size	0.8 m × 0.8 m × 0.2 m	40 m × 40 m × 10 m

Four groups of imaging results are also shown in Fig. 5, and their layout is consistent with Fig. 4. From the four sets of imaging results of 100 km scaling training, it can be seen that although the contour information of the target can also be accurately inverted, the accuracy of depth information inversion is lower than that of 10 km. This is because the distance of 100 km is increased by 10 times compared with 10 km while the 3-D plane target size is unchanged, and the pulse width and time bin are the same in the two simulations.

According to (3) and (11), the echo signal of the long-distance scene to be imaged and parameter scaling system have the same magnitude and envelope, but their exponential terms differ by a scaling factor. While the pulse width are comparable to or even smaller than the time resolution (approximate to the detector time bin in this simulation), their difference in scaling factor can be ignored. Therefore, the mapping relationship between the 3-D scene and photon-counting histogram will be closer in these two system. In order to prove this hypothesis, the following simulations are carried out: according to the parameters in Table II, the time bin is set to 50 ps, and the pulse width is taken as 1–5 times of it for scaling training. As shown in Fig. 6, normalized mean square error (NMSE) and structural similarity

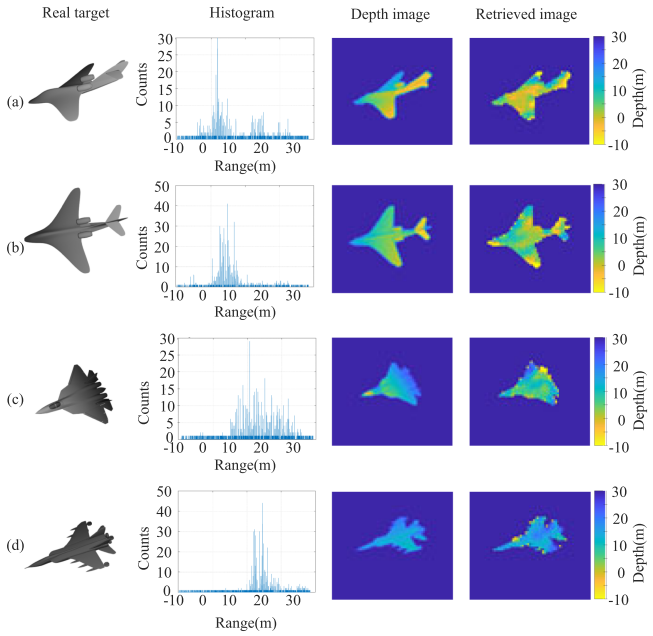

Fig. 4. Imaging results of 10 km. The "0" in the axes of histograms and the depth colorbars represent 10 km.

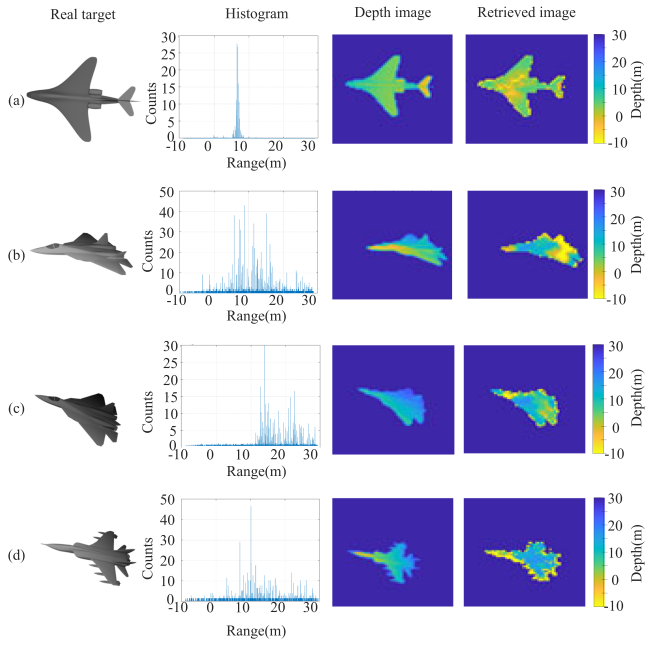

Fig. 5. Imaging results of 100 km. The "0" in the axes of histograms and the depth colorbars represent 100 km.

(SSIM) [29] index are calculated for the imaging results under five different simulations to evaluate the quality of the retrieved images.

In Fig. 6, it can be seen the larger the T_{p}/t_s, the worse the quality of the retrieved images. Fig. 7(a) and (b) shows the comparison of photon-counting histograms of the same target in long-distance scene and parameters scaling system at $T_{\mathrm{p}}/t_s = 1$ and $T_{\mathrm{p}}/t_s = 5$, respectively. When $T_{\mathrm{p}}/t_s = 1$, the peak position

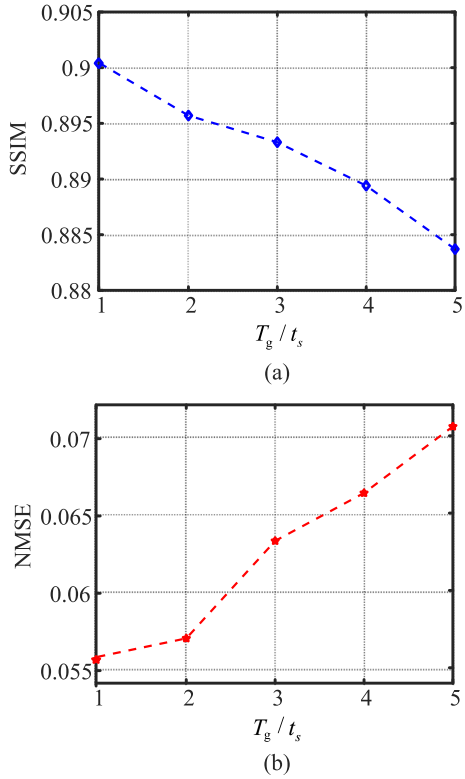

Fig. 6. Reconstruction performance curve of the scaling training method under different T_{p}/t_s. (a) SSIM curve. (b) NMSE curve.

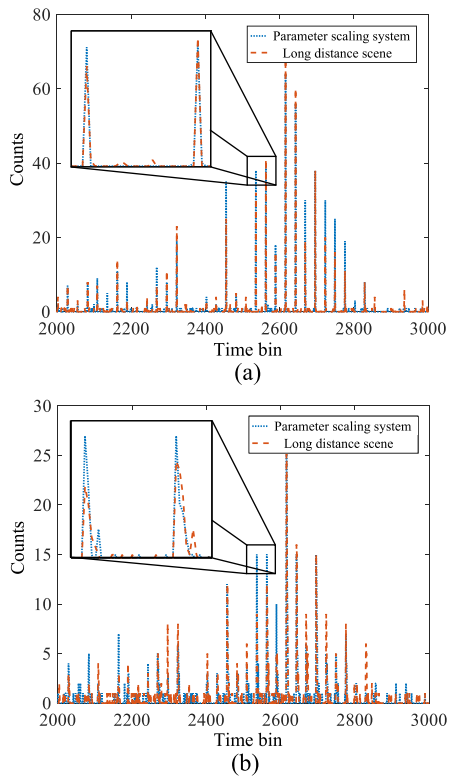

Fig. 7. Comparison of photon-counting histograms with different parameters. (a) Photon-counting histogram of $T_{\mathrm{p}}/t_s = 1$. (b) Photon-counting histogram of $T_{\mathrm{p}}/t_s = 5$.

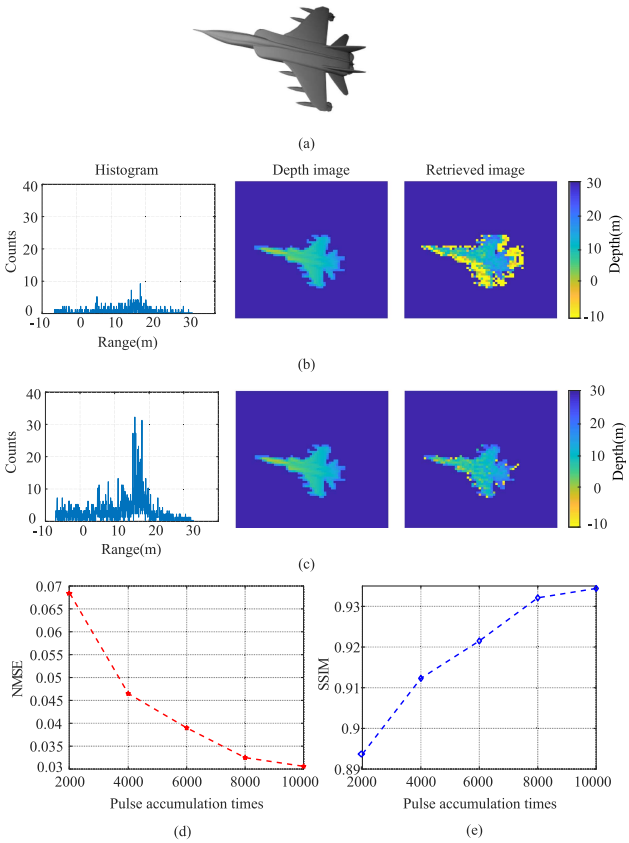

Fig. 8. Imaging results of different pulse accumulation times. (a) Original targets. (b) Result of 2000 times pulse accumulation. (c) Result of 10 000 times pulse accumulation. (d) SSIM curve. (e) NMSE curve. The "0" in the axes of histograms and the depth colorbars represent 10 km.

and envelope of the photon-counting histogram of these two are almost the same, and there are only slight differences in a few fluctuations due to the random distribution of the echo photons. When $T_{\mathrm{p}}/t_s = 5$, it is found that the envelope and peak position of both have a large deviation, which is caused by the scaling factor. Hence, setting the pulse width to be less than or equal to the time resolution of the detector will obviously improve the imaging quality. This is the reason why $T_{\mathrm{p}}/t_s = 1$ in the former simulations.

For long-distance detection and imaging, the signal-to-noise ratio is an important parameter. In terahertz single-photon radar system, it is mainly affected by the number of pulses accumulation times. To investigate the influence of pulse accumulation times on imaging quality, the pulse accumulation times from 2000 to 10 000 with 2000 intervals were taken into consideration in the simulations and other conditions are remain unchanged. The results are summarized in the figures as follows. From the results, it is found that when the pulse accumulation times is 10 000, the target contour information and depth information can be reconstructed successfully, while when the pulse accumulation times is 2000, there are many pseudoscattering points, and the depth information is no longer accurate. Fig. 8(d) and (e), respectively, shows the MSE and SSIM while changing the pulse accumulation times. Without surprise, the imaging quality degrades as the pulse accumulation times decreases.

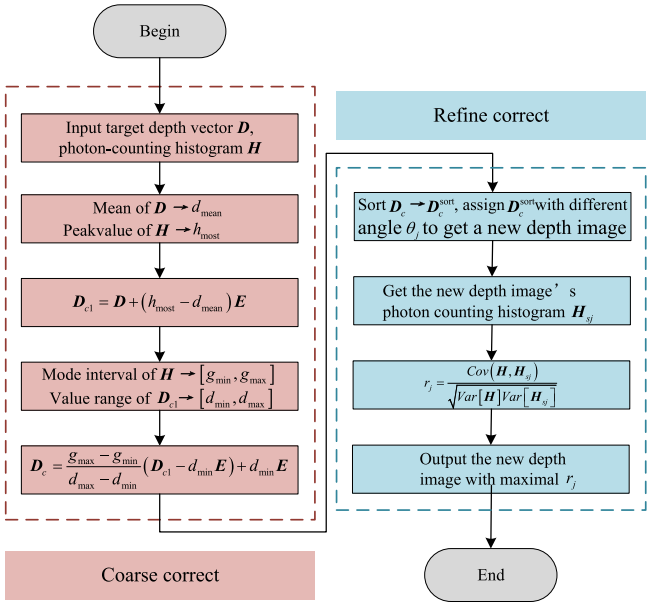

Fig. 9. Flow chart of the depth correction.

IV. Depth Correction

Obviously, the higher the time resolution of the detector, the better the imaging quality. However, restricted by physics limits, the time resolution cannot be improved infinitely. In Section III, although the scaling training method is implemented in imaging the target with the size of 40 m × 40 m × 20 m at 100 km, the inversion of depth information is inaccurate. Thus, to further mine the information in photon-counting histogram and improve the imaging quality, we propose a depth correction method.

This method has two steps, including coarse correction and refined correction. The purpose of coarse correction is to correct some points with large deviation or even beyond the range into the range gate. This step will serve as the basis for subsequent refined correction.

First, separate the target point from the background, since the background has no significance for correction. Assume that the target points to be corrected are Q, the vector formed by the depth of each point is $\boldsymbol{D} = [d_1, d_2, \ldots, d_q, \ldots d_Q]$, the mean value of $\boldsymbol{D}$ is d_{mean}. And the photon-counting histogram of the target is $\boldsymbol{H}$, the distance corresponding to the point with the highest peak in $\boldsymbol{H}$ is h_{most}. Based on that, the first step of coarse correction can be represented as

$$\boldsymbol{D}_{c1} = \boldsymbol{D} + (h_{\mathrm{most}} - d_{\mathrm{mean}})\,\boldsymbol{E} \tag{12}$$

where the elements in vector $\boldsymbol{E}$ are all 1, and the dimension is the same as $\boldsymbol{D}$. This step can make the overall depth value of the target closer to the distance corresponding to the peak value of the photon-counting histogram, that is, the position where the most target points are located at this distance, then scale the point from the outside to the inside of the range gate. A decision threshold T is set first, the threshold T is to decide the distance interval where most target points are located, it is utilized to filter out noise and some very weak scattering points that may be present. In general, the threshold T is set to the mean value

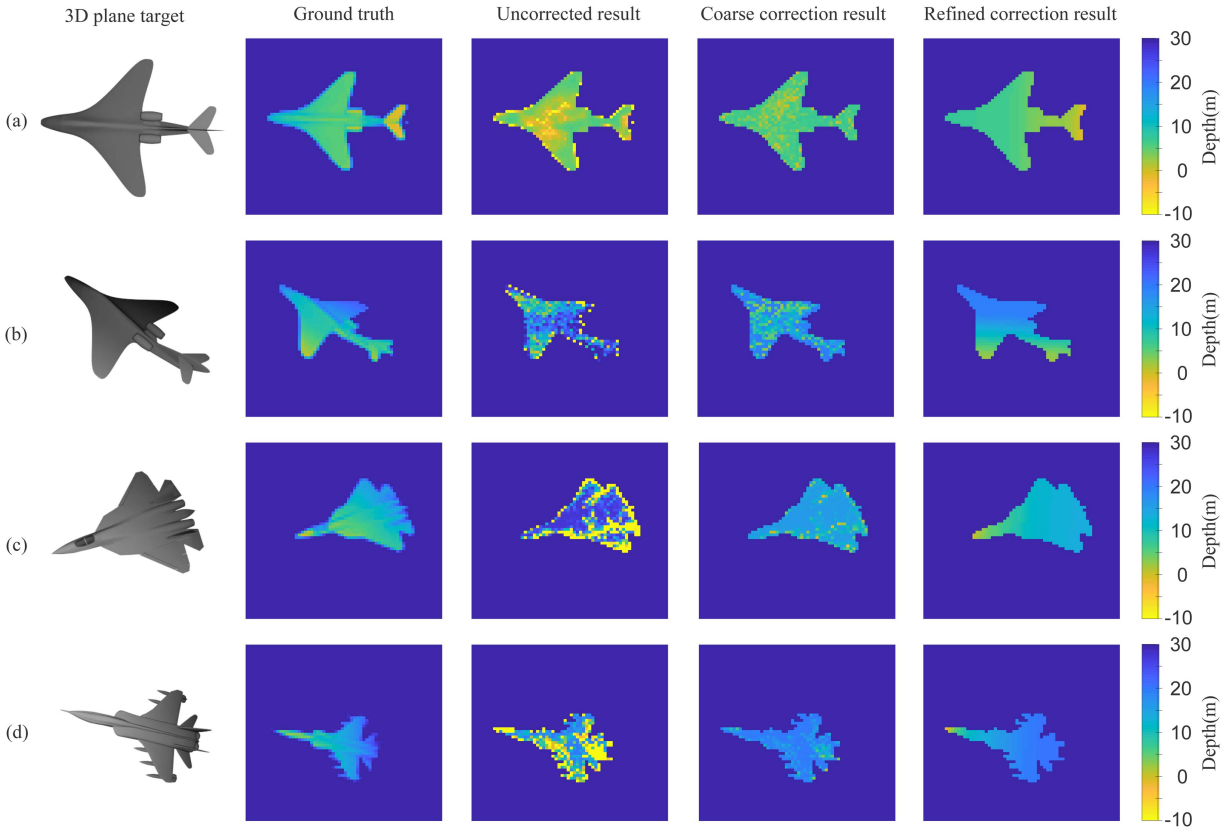

Fig. 10. Depth correction results. The "0" in the depth colorbar represents 100 km. (a) The depth correction results of target 1; (b) The depth correction results of target 1 in different attitude; (c) The depth correction results of target 2; (d) The depth correction results of target 3.

of the photon-counting histogram, and it is worth noting that the 0 count value needs to be culled. By comparing the count value of each time bin in $\boldsymbol{H}$ with T, take the first time bin and the last time bin greater than T as the range of the distance interval $[g_{\min}, g_{\max}]$ where most target points are located. Then, calculate the minimum $d_{\min}$ and maximum $d_{\max}$ of $\boldsymbol{D}_{c1}$. The specific scaling method is as follows:

$$\boldsymbol{D}_c = \frac{g_{\max} - g_{\min}}{d_{\max} - d_{\min}} \left(\boldsymbol{D}_{c1} - d_{\min}\boldsymbol{E}\right) + d_{\min}\boldsymbol{E}. \tag{13}$$

The next step will be refined correction based on coarse correction. Since the detection range of terahertz single-photon radar is generally as far as tens of kilometers or even hundreds of kilometers, the fine structure on the target under this imaging range is no longer important. The more practical significance should be to judge the attitude, and obtain the target's movement direction and other information through the depth comparison and change trend of different parts of the target. The detailed operation of refine correction is as follows. First, divide the circumference into J intervals according to the actual application requirements, and the central angle of each interval is $\theta_j, j = 1, 2, \ldots J$. Then, sort the elements of $\boldsymbol{D}_c$ from small to large to get $\boldsymbol{D}_c^{\text{sort}}$. For each θ_j, starting from the direction of the target's line of sight at that angle, assign the depth value in $\boldsymbol{D}_c^{\text{sort}}$ to each target point in the depth image after coarse correction to obtain a new depth image. Then, get the photon-counting histogram of the new depth image marked as $\boldsymbol{H}_{sj}$ according to terahertz single-photon echo model, and calculate

$$r_j = \frac{\text{Cov}\left(\boldsymbol{H}, \boldsymbol{H}_{sj}\right)}{\sqrt{\text{Var}\left[\boldsymbol{H}\right] \text{Var}\left[\boldsymbol{H}_{sj}\right]}}, j = 1, 2, \ldots, J \tag{14}$$

where $\text{Cov}(\boldsymbol{H}, \boldsymbol{H}_{sj})$ is the covariance between $\boldsymbol{H}$ and $\boldsymbol{H}_{sj}$, $\text{Var}[\boldsymbol{H}]$ and $\text{Var}[\boldsymbol{H}_{sj}]$ are the variance of $\boldsymbol{H}$ and $\boldsymbol{H}_{sj}$, respectively. The similarity between $\boldsymbol{H}$ and $\boldsymbol{H}_{sj}$ is measured by the correlation coefficient r_j. The larger the correlation coefficient, the more similar these two, which means that the depth image corresponding to $\boldsymbol{H}_{sj}$ is closer to the true depth image, so as to achieve the purpose of correction. The flow chart of the depth correction is shown in Fig. 9.

To demonstrate the feasibility of the proposed depth correction method, the imaging results of several different models and attitudes at 100 km were utilized for implementation. The depth correction results are shown in Fig. 10. There are five columns pictures in total, including the real targets, ground-truth depth images, uncorrected depth images, coarse correction depth images, and refined correction depth images. It can be seen that the uncorrected results are accurate in the contour information, but there are many noise points in the middle, and it is difficult to recognize the far and near relationship of each part of the plane targets, so it is difficult to judge the attitude. After coarse correction, the noise is eliminated, and the error points at the edges are corrected, but the attitude angle of the plane targets is still not intuitive. While after refined correction, the brightness

of different parts of the planes indicates its depth (the distance away from detector), from which the planes flying attitude can be judged and is consistent with the plane target's attitude in the ground-truth depth image.

V. Conclusion

In this article, a forward-looking 3-D imaging method based on terahertz single-photon radar for long-distance applications has been proposed. The imaging method is based on SISO architecture system and adopts data-driven approach. To solve the limitations of data collection in long-distance applications, we propose a scaling training method and verify its feasibility through simulations. On this basis, to further improve the imaging quality, the depth correction method is implemented and the simulation results prove its effectiveness. Different from the existing detector arrays or mechanical scanning schemes, the proposed imaging method is compact and cost-effective. It has great potential in many applications, such as long-distance warning, stealth target detection, and imaging.

References

[1] F. Gan, C. Luo, H. Wang, and B. Deng, "Robust compressive terahertz coded aperture imaging using deep priors," *IEEE Geosci. Remote Sens. Lett.*, vol. 19, Feb. 2022, Art. no. 3511205, doi: 10.1109/LGRS.2022.3150921.

[2] X. Chen, H. Wang, Q. Yang, Y. Zeng, and B. Deng, "An efficient mmW frequency-domain imaging algorithm for near-field scanning 1-D SIMO/MIMO array," *IEEE Trans. Instrum. Meas.*, vol. 71, Jul. 2022, Art. no. 8004612, doi: 10.1109/TIM.2022.3189631.

[3] Y. Cheng, L. Qiao, D. Zhu, Y. Wang, and Z. Zhao, "Passive polarimetric imaging of millimeter and terahertz waves for personnel security screening," *Opt. Lett.*, vol. 46, no. 6, pp. 1233–1236, 2021.

[4] Z. Ou, J. Wu, H. Geng, X. Deng, and X. Zheng, "Confocal terahertz SAR imaging of hidden objects through rough-surface scattering," *Opt. Exp.*, vol. 28, pp. 12405–12415, 2020.

[5] P. H. Siegel, "Terahertz technology," *IEEE Trans. Microw. Theory Techn.*, vol. 50, no. 3, pp. 910–928, Mar. 2002.

[6] C. Jansen et al., "Terahertz imaging: Applications and perspectives," *Appl. Opt.*, vol. 49, no. 19, pp. E48–E57, 2010.

[7] K. Kawase, Y. Ogawa, Y. Watanabe, and H. Inoue, "Non-destructive terahertz imaging of illicit drugs using spectral fingerprints," *Opt. Exp.*, vol. 11, no. 20, pp. 2549–2554, 2003.

[8] S. Kim, R. Fan, and F. Dominski, "ViSAR: A 235GHz radar for airborne applications," in *Proc. IEEE Radar Conf.*, 2018, pp. 1549–1554.

[9] S. Komiyama, "Single-photon detectors in the terahertz range," *IEEE J. Sel. Topics Quant Electron.*, vol. 17, no. 1, pp. 54–66, Jan./Feb. 2011.

[10] Z. Wang, T. Nakajima, S. Matsuda, and S. Komiyama, "A new scheme for sensitive detection of terahertz photons," *Nanotechnology*, vol. 24, no. 2, 2012, Art. no. 025205.

[11] J Bueno, M. D. Shaw, P. K. Day, and P. M. Echternach, "Proof of concept of the quantum capacitance detector," *Appl. Phys. Lett.*, vol. 96, no. 10, 2010, Art. no. 103503.

[12] P. Echternach et al., "Photon shot noise limited detection of terahertz radiation using a quantum capacitance detector," *Appl. Phys. Lett.*, vol. 103, no. 5, 2013, Art. no. 53510.

[13] P. Echternach, B. Pepper, T. Reck, and C. Bradford, "Single photon detection of 1.5 THz radiation with the quantum capacitance detector," *Nature Astron.*, vol. 2, pp. 90–97, 2017.

[14] K. Liu, C. Luo, J. Yi, and H. Wang, "Target detection method using heterodyne single-photon radar at terahertz frequencies," *IEEE Geosci. Remote Sens. Lett.*, vol. 19, 2022, Art. no. 3505605.

[15] K. Liu, Z. Gong, and J. Yi, "Direct-detection single-photon radar at terahertz frequencies," in *Proc. 13th Glob. Symp. Millimeter-Waves THz*, 2021, pp. 1–3.

[16] Z. Li et al., "Single-photon computational 3D imaging at 45km," *Photon. Res.*, vol. 9, pp. 1532–1540, 2020.

[17] Z. Li et al., "Single-photon imaging over 200km," *Optica*, vol. 8, no. 3, pp. 344–349, 2021.

[18] R. Lussana, F. Villa, A. Mora, D. Contini, A. Tosi, and F. Zappa, "Enhanced single-photon time-of-flight 3D ranging," *Opt. Exp.*, vol. 23, no. 19, pp. 24962–24973, 2015.

[19] A. Pawlikowska, A. Halimi, R. Lamb, and G. Buller, "Single-photon three-dimensional imaging at up to 10 kilometers range," *Opt. Exp.*, vol. 25, no. 10, pp. 11919–11931, 2017.

[20] A. Turpin et al., "Spatial images from temporal data," *Opt. Exp.*, vol. 7, no. 8, pp. 900–905, 2020.

[21] C. Liang, C. Luo, B. Deng, K. Liu, and F. Gan, "Non-scanning SISO 3D imaging of terahertz single-photon radar," in *Proc. Int. Conf. Microw. Millimeter Wave Technol.*, 2022, pp. 1–3.

[22] G. Bouquet, J. Thorstensen, K. Bakke, and P. Risholm, "Design tool for TOF and SL based 3D cameras," *Opt. Exp.*, vol. 25, no. 22, pp. 27758–27769, 2017.

[23] S. May et al., "Three-dimensional mapping with time-of-flight cameras," *J. Field Robot.*, vol. 26, no. 11, pp. 934–965, 2009.

[24] Y. Lecun, Y. Bengio, and G. Hinton, "Deep learning," *Nature*, vol. 521, no. 7553, pp. 436–444, 2015.

[25] T. Poggio and F. Girosi, "Networks for approximation and learning," *Proc. IEEE*, vol. 78, no. 9, pp. 1481–1497, Sep. 1990.

[26] C. M. Bishop, "Neural networks for pattern recognition," *Adv. Comput.*, vol. 37, pp. 119–166, 1993.

[27] C. Liang, C. Luo, B. Deng, Z. Yang, H. Wang, and F. Gan, "Non-scanning SISO terahertz 3D imaging based on data-driven," *Opt. Exp.*, vol. 30, no. 16, pp. 29329–29339, 2022.

[28] B. R. Mahafza, *Radar System Analysis and Design Using Matlab*. Boca Raton, FL, USA: Chapman and Hall, 2005.

[29] Z. Wang, A. C. Bovik, H. R. Sheikh, and E. P. Simoncelli, "Image quality assessment: From error visibility to structural similarity," *IEEE Trans. Image Process.*, vol. 13, no. 4, pp. 600–612, Apr. 2004.

Chuanying Liang was born in Hubei Province, China, in 1999. He received the B.S. degree in information and communication engineering in 2022 from the National University of Defense Technology (NUDT), Changsha, China, where he is currently working toward the Ph.D. degree in information and communication engineering.

His research interests include terahertz radar imaging, radar waveform design, and signal processing.

Chenggao Luo received the Ph.D. degree in optical engineering from Sichuan University, Chengdu, China, in 2015.

He has been a Visiting Research Scholar with the University of Connecticut, Storrs, CT, USA, from 2012 to 2013. He is currently an Associate Professor with the College of Electronic Science and Technology, National University of Defense Technology, Changsha, China. His recent research interest includes optical 3-D imaging and display, terahertz imaging, and coded-aperture imaging.

Jun Yi received the B.S. degree in physical electronics from the University of Electronic Science and Technology of China (UESTC), Chengdu, China, in 2014 and the Ph.D. degree in electronical science and technology from Hunan University (HNU), Changsha, China, in 2019.

He is currently a Lecturer with the College of Electronic Science and Technology, National University of Defense Technology, Changsha, China. His research interests include terahertz radar system and terahertz-wave high-sensitive detection technology. His recent research interest includes optical 3-D imaging and display, terahertz imaging, and coded-aperture imaging.

Bin Deng was born in Shandong, China, in 1980. He received the B.S. degree in information and communication engineering from Northeastern University, Shenyang, China, in 2004 and the M.S. and Ph.D. degrees in information and communication engineering from the National University of Defense Technology (NUDT), Changsha, China, in 2006 and 2011, respectively.

He is currently an Associate Professor with the School of Electronic Science and Technology, NUDT. His research interests include synthetic aperture radar (SAR), SAR/ground moving target indication, and terahertz radar.

Hongqiang Wang was born in Shaanxi Province, China, in 1970. He received the B.S., M.S., and Ph.D. degrees in information and communication engineering from the National University of Defense Technology (NUDT), Changsha, China, in 1993, 1999, and 2002, respectively.

He is currently a Professor with the College of Electronic Science and Technology, NUDT. He has been involved in modern radar signal processing research and development since 1996. His research interests include automatic target recognition, radar imaging, and target tracking.

Kang Liu was born in Siyang, China. He received the B.S. degree in information and communication engineering from the Nanjing University of Aeronautics and Astronautics, Nanjing, China, in 2012 and the M.S. and Ph.D. degrees in information and engineering from the National University of Defense Technology, Changsha, China, in 2014 and 2017, respectively.

From 2016 to 2017, he was a Visiting Ph.D. Student with the Queen Mary University of London, London, U.K. He is currently an Associate Professor of Signal Processing with the National University of Defense Technology. His research interests include electromagnetic (EM) vortex, radar imaging, and quantum radar.

Qi Yang was born in Shaanxi Province, China, in 1989. He received the B.S., M.S., and Ph.D. degrees in information and communication engineering from the National University of Defense Technology (NUDT), Changsha, China, in 2012, 2014, and 2018, respectively.

He is currently an Associate Professor with the College of Electronic Science and Technology, NUDT. His research interests include terahertz radar system and signal processing of ISAR.